INTERNATIONAL JOURNAL OF
ENERGY AND ENVIRONMENT

Volume 3, Issue 2, 2012 pp.247-266

Journal homepage: www.IJEE.IEEFoundation.org

A computational study to investigate the effects of insulation and EGR in a diesel engine

Syed Yousufuddin[1], K.Venkateswarlu[2], Naseeb Khan[3]

[1] Department of Mechanical Engineering, Jubail University College, Royal Commission - Jubail , P.O. Box 10074, Jubail Industrial City- 31961, Kingdom of Saudi Arabia.
[2] Department of Mechanical Engineering, K.L University Vaddeswaram, Guntur(Dist), Andhra Pradesh - 522502, India.
[3] Shaaz College of Engg. & Tech. Himayatnagar, Moinabad Mandal, Ranga Reddy (Dist) - 500 075, Andhra Pradesh, India.

Abstract
Higher heat losses and brake specific fuel consumption (BSFC) are major problems in an indirect injection (IDI) diesel engine, which can be overcome by means of insulation. However, insulation increases combustion temperature by about 200-250^0 compared to an identical standard IDI diesel engine. Consequently, the NO_x emission increases extremely due to this temperature increment. With the proper adjustment of cold EGR mass fraction, it is possible to partially offset the adverse effect of insulation on heat release rate and hence to obtain improved performance and lower NO_x than the baseline engine. At the first step of this work, the effects of insulation (without heat flux) on the performance and emissions are studied at both part and full loads by a three dimensional model. The results show that in the adiabatic case, BSFC is approximately 18% and 23% lower than baseline at the full and part loads respectively. Also, soot emission shows 36% reduction at full load, while at the part load, the value of which remains unchanged. At the second step of the present work, for reduction of NO_x production in the insulated engine, cold exhaust gas recirculation (EGR) method is utilized. Thus, the model is studied at various cold EGR mass fractions, in which the EGR mass fraction increases from 0% to 30% at the same speed and operating loads. The optimum cold EGR mass fraction is obtained as 10% for part load operation. Results show that with adding this optimum EGR, the BSFC and NO_x decrease by 15% and 6.5 % respectively at full load compared to the baseline and these reductions are reached to 21% and 29% in the case of part load respectively, while it causes increment in soot emission at full load operation and decreases slightly in the part load compared to the baseline engine. As an engine is generally operated for a short time interval at full load condition, this increment can be omitted when improvements in BSFC and decrease in NO_x are considered together. The results of the model for baseline engine are in good agreement with the corresponding experimental data. This agreement makes the model a reliable tool that can be used for exploring new engine concepts.

Keywords: Adiabatic; Emission; Indirect injection; NO_x; Soot.

1. Introduction

Combustion characteristics of an engine are very important parameters for interpreting engine performance and exhaust emissions. They are also useful for engine design and optimization. Besides, the combustion characteristics such as maximum cylinder gas pressure ,temperature and heat-release rate can be used to explain the effects of engine-operating conditions on the performance or can be used as fundamental parameters for comparing various alternative fuels under the same operating conditions [1-3]. The combustion characteristics of the (IDI) engines are different from (DI) engines, because of high turbulence intensity and greater heat-transfer losses in the swirl chamber [4]. This defect causes the brake-specific fuel consumption (BSFC) of the IDI engine to increase and the total engine efficiency to decrease compared to that of a DI diesel engine. Because of these disadvantages of the IDI diesel engines, most engine research has focused on the DI diesel engines. However, because of higher air velocity and rapidly occurring air-fuel mixture formation in both combustion chambers of the IDI diesel engines, these engines have a simple fuel injection system and lower injection pressure level [5, 6]. In addition, they do not depend upon the fuel quality [5, 6] and produce lower exhaust emissions [7] than DI diesel engines. Especially, unburned hydrocarbon (HC) and carbon monoxide (CO) emissions were significantly lower in these engines, which have homogeneous charge condition [8, 9]. The concept of low heat rejection (LHR) engine aims to reduce the great heat loss transferred to cooling system in an IDI engine. So, this energy can be converted to useful work [10]. Some of the major advantages of LHR engines include better fuel economy, increased engine life, reduction in HC, CO and PM emissions, and lower combustion noise due to reduced pressure increasing rate, increased exhaust gas exergy, and ability of operating lower cetane fuels [11-17]. Also, the higher temperatures in the combustion chamber can have a positive effect on diesel engines at adiabatic case, due to the self-ignition delay drop [18]. A lot of experimental study has been done to utilize LHR engine concept to improve thermal efficiency by reducing heat losses, and to improve mechanical efficiency by eliminating cooling systems. The experimental investigations of Adnan Parlak et al. and Ekrem Buyukkaya et al. [19, 20] revealed that with the proper adjustment of the injection timing, it is possible to partially offset the adverse effect of insulation on heat release rate and hence to obtain improved performance and lower NO_x. Dickey performed experimental investigation [21] on insulated engines and showed that shorter ignition delay, decreased premixed fraction and a corresponding increase in the amount of fuel burned during the diffusion phase of combustion were observed in the case of LHR engine. The experiments of S. Jaichandar et al. [22] show that high temperature operation of LHR causes considerable improvement in fuel consumption and thermal efficiency, increased availability in the exhaust gas and NOx formation, a reduction of soot formation. The main factors of influence on the NO_x emissions produced by the combustion process are stoichiometric equivalence ratio and flame temperature. However, Because of the diffusive mixing of air and fuel occurring along the spray envelope, combustion is dominated by near-stoichiometric burning, where production of nitric oxide is high [23]. According to Yiming Wang et al. [24], the characteristics of high temperature combustion, the methods, such as decreasing hole diameter, optimizing injection timing and employing a special type of impingement plate in the combustion chamber which breaks the envelope of high temperature flame, can reduce the combustion duration , achieve high efficiency and low soot emission in LHR engines. Also an experimental investigation on the effect of ceramic coatings on diesel engine performance and exhaust emissions which was performed by Dennis Assanis et al. [25] shows that in the optimum thickness of ceramic coating, efficiency increases 10%, exhaust CO levels were between 30% and 60% lower than baseline levels and unburned HC levels were 35% to 40% lower for the insulated pistons. Also the NO_x concentrations were also 10% to 30% lower due to the changed nature of combustion in the insulated engines. Finally, smoke emissions decreased slightly in the insulated engines.

Numerical studies about energy and exergy of exhaust gas stream, which is the most important source of available energy and exergy in a LHRE, have been performed by many authors [26-29] at the optimum injection timing and have shown that lower heat rejection from the combustion chamber through thermally insulated components causes an increase in available energy that would increase the in-cylinder work and the amount of energy carried by the exhaust gases, which could also be utilized. Many fundamental aspects concerning of CFD simulation of IDI engines have been discussed earlier by Pinchon [30]. Three dimensional modeling of combustion process and soot formation in an indirect injection diesel engine using KIVA CFD code have been progressed by Zellat [31]. Strauss and Schweimer [32], at Volkswagen AG, studied the combustion and pollutant formation processes in a 1.9 l IDI diesel engine using SPEED CFD code for a part and full load. The global properties are presented

resolved for the swirl and main chamber and the swirl chamber throat separately. Also, the thermal NO_x and soot formation are simulated and analyzed as well [32]. In fact, it is now commonly admitted that the design of IDI combustion chambers has to rely increasingly more on fundamental knowledge of local aspect requiring multidimensional simulation. As can be seen in the relevant literature, there are a few attempts about using three dimensional modeling for finding the optimization state at adiabatic IDI diesel engines up to now. In this present work, a CFD model has been used to predict flow field, combustion process and emissions in the Lister 8.1 indirect injection diesel engine in baseline, adiabatic, and adiabatic with EGR conditions. For optimization and simultaneously improvement of NO_x emission and performance at the adiabatic case, EGR applying method is used at both full and part loads. The EGR percentage (EGR %) in this study was varied from 0% to 30%.

2. Problem formulation

2.1 Initial and boundary conditions

Calculations are carried out on the closed system from intake valve closure (IVC) at 165°CA BTDC to exhaust valve open (EVO) at 125°CA ATDC. Figure 1 shows the numerical grid, which is designed to model the geometry of the combustion chamber engine and contains a maximum of 42200 cells at 165°CA BTDC. It captures features like the glow plug channel, the piston and the swirl chamber throat. The present resolution was found to give adequately grid independent results. A single hole injector is mounted in pre-chamber as shown in Figure 2. Initial pressure in the combustion chamber is set to 86 kPa and initial temperature is calculated to be 384K. The Present work includes study of three operating conditions of engine: base line, adiabatic and also adding EGR to the initial charge of adiabatic case at two load operating conditions: a full load and a part load (50% load). At all the cases, engine speed is 730rev/min. All the wall boundaries temperatures were assumed to be constant throughout the simulation in base mode, but allowed to vary with the combustion chamber surface regions. In adiabatic case, all boundaries were assumed to be without heat flux. In EGR case 0% to30% of EGR mass fraction was added to the inlet charge and it is assumed that EGR temperature is equal with temperature of inlet charge (cold EGR).

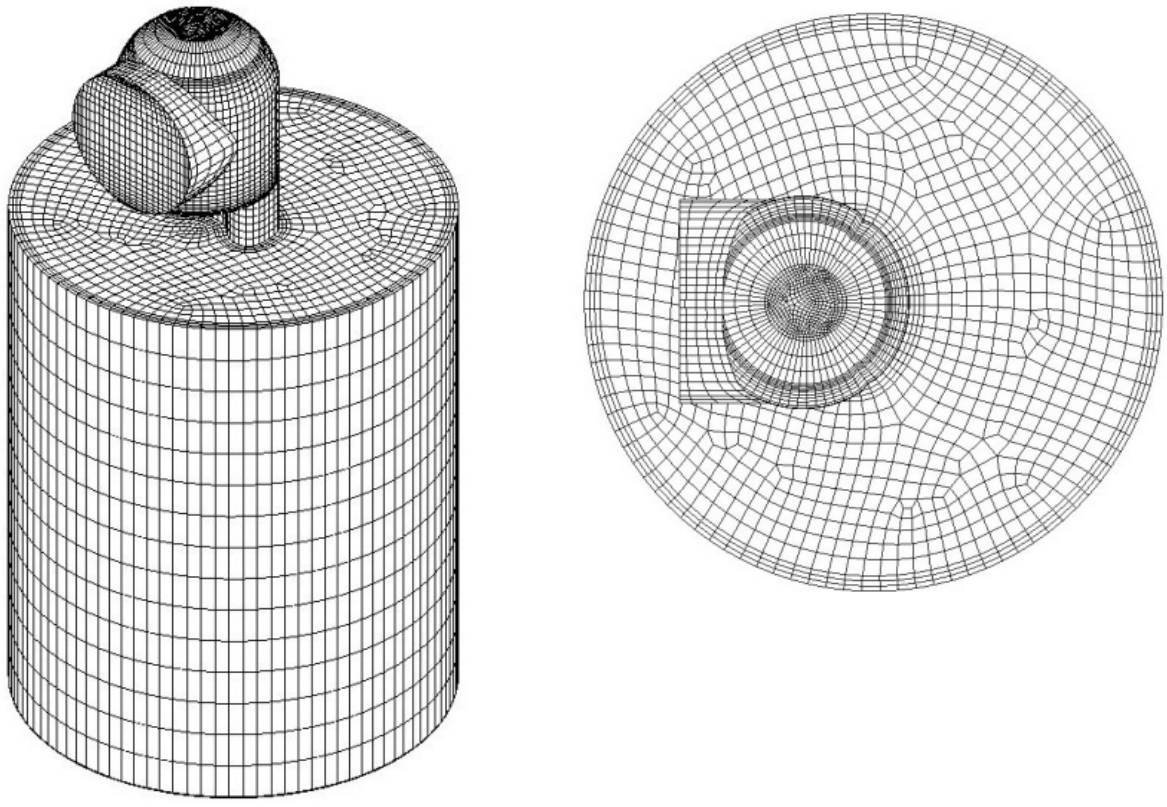

(a) (b)

Figure 1. (a) Mesh of the Lister 8.1 indirect injection diesel engine, (b) Top view of the mesh

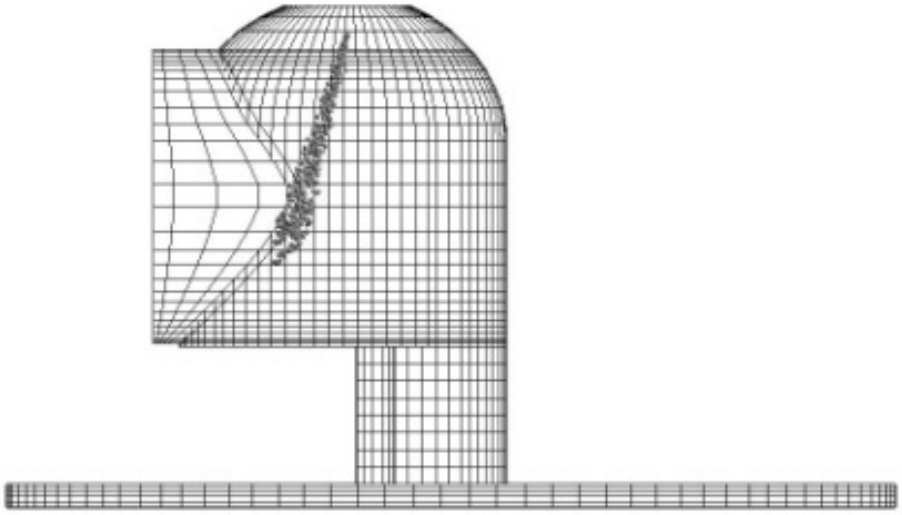

Figure 2. Spray and Injector coordinate at pre-chamber

2.2 Model formulation

The numerical model is carried out for Lister 8.1 indirect injection diesel engine with the specifications shown in Table 1. The governing equations for unsteady, compressible, turbulent reacting multi-component gas mixtures flow and thermal fields were solved from IVC to EVO by the commercial AVL-FIRE CFD code [33]. The turbulent flows within the combustion chamber are simulated using the RNG $k-\varepsilon$ turbulence model, modified for variable-density engine flows [34]. The standard WAVE model, described in [35], is used for the primary and secondary break up modeling of the resulting droplets. At this model, the growth of an initial perturbation on a liquid surface is linked to its wave length and other physical and dynamical parameters of the injected fuel at the flow domain. Drop parcels are injected with characteristic size equal to the Nozzle exit diameter (blob injection). The injection rate profiles at the full and 50% loads are shown in Figure 3. The Dukowicz model is applied for treating the heat up and evaporation of the droplets, which is described in [36]. This model assumes a uniform droplet temperature. In addition, the droplet temperature change rate is determined by the heat balance, which states that the heat convection from the gas to the droplet either heats up the droplet or supplies heat for vaporization. A Stochastic dispersion model was employed to take the effect of interaction between the particles and the turbulent eddies into account by adding a fluctuating velocity to the mean gas velocity [37]. This model assumes that the fluctuating velocity has a randomly Gaussian distribution. The spray/wall interaction model used in this simulation was based on the spray/wall impingement model [38]. This model assumes that a droplet, which hits the wall is affected by rebound or reflection based on the Weber number. The Shell auto-ignition model was used for modeling of the auto ignition [39]. In this generic mechanism, 6 generic species for hydrocarbon fuel, oxidizer, total radical pool, branching agent, intermediate species and products were involved. In addition the important stages of auto ignition such as initiation, propagation, branching and termination were presented by generalized reactions, described in [33, 39]. The Eddy Break-up model (EBU) based on the turbulent mixing was used for modeling of the combustion process in the combustion chamber [33] as follows:

$$\overline{\rho \dot{r}_{fu}} = \frac{C_{fu}}{\tau_R} \bar{\rho} \min\left(\bar{y}_{fu}, \frac{\bar{y}_{ox}}{S}, \frac{C_{pr} \cdot \bar{y}_{pr}}{1+S} \right) \tag{1}$$

where this model assumes that in premixed turbulent flames, the reactants (fuel and oxygen) are contained in the same eddies and are separated from eddies containing hot combustion products. The rate of dissipation of these eddies determines the rate of combustion. In other words, chemical reaction occurs fast and the combustion is mixing controlled .The first two terms of the "minimum value of" operator determine whether fuel or oxygen is present in limiting quantity, and the third term is a reaction probability which ensures that the flame is not spread in the absence of hot products. Above equation includes three constant coefficients (C_{fu}, τ_R, C_{pr}) and C_{fu} varies from 3 to 25 in diesel engines. An optimum

value was selected according to experimental data [33, 40]. NO_x formation is modeled by the Zeldovich mechanism and Soot formation is modeled by Kennedy, Hiroyasu and Magnussen mechanism [41].

Table 1. Specifications of Lister 8.1 IDI diesel engine

Cycle Type	Four Stroke
Number of Cylinders	1
Injection Type	IDI
Cylinder Bore	114.1 mm
Stroke	139.7 mm
L/R	4
Displacement Volume	1.43 lit.
Compression Ratio	17.5 : 1
$V_{pre\text{-}chamber}/V_{TDC}$	0.7
Full Load Injected Mass	$6.4336e-5$ Kg per Cycle
Part Load Injected Mass	$3.2009e-5$ Kg per cycle
Max Power on 850 rpm	8 hp
Max Power on 650 rpm	6 hp
Injection Pressure	91.7 kg/cm^3
Start Injection Timing	20° BTDC
Nuzzle Diameter at Hole Center	0.003m
Number of Nuzzle Holes	1
Nuzzle Outer diameter	0.0003m
Spray Cone Angle	10°
Valve Timing	IVO= 5° BTDC IVC= 15° ABDC EVO= 55° BBDC EVC= 15° ATDC

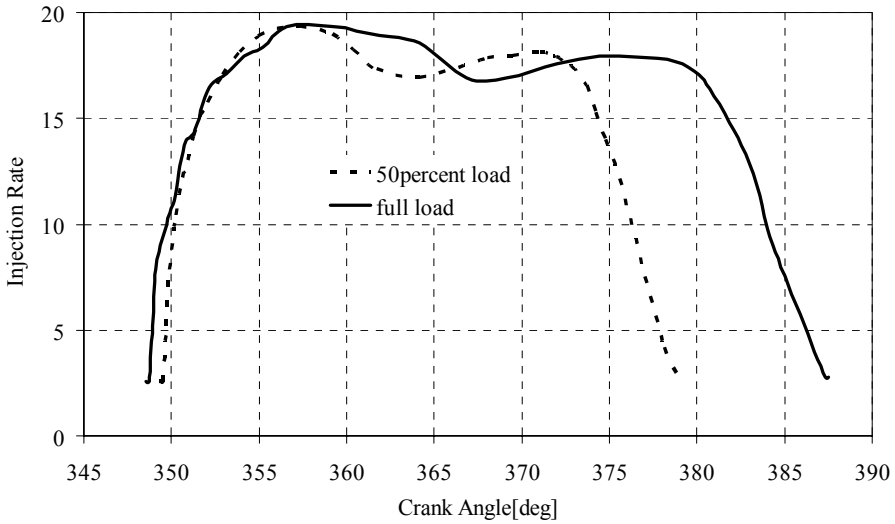

Figure 3. Part and full load injection histories

3. Results and discussion

The calculations are carried out for the single cylinder Lister 8.1 IDI Diesel engine and the operating conditions are both full and 50% load at constant speed of 730 rev. /min. Figures 4 and 5 show the comparison of computed and measured [40] mean in-cylinder pressure and Heat Release Rate (H.R.R) respectively for both loads. The results presented in those figures are global (cylinder averaged) quantities as a function of time (crank angle). The measured heat release rate curve is derived from the first law analysis of procured in-cylinder pressure data as follows:

$$\frac{dq}{d\theta} = \frac{\gamma}{\gamma - 1} p \frac{dV}{d\theta} + \frac{1}{\gamma - 1} V \frac{dp}{d\theta} \tag{2}$$

In the above equation, p and V are in-cylinder pressure and volume vs. crank angle θ, and $\gamma = 1.35$.

The good agreement between measured and predicted data especially during the compression, start of combustion and expansion strokes verifies the model. Also Peak values for both premixed and diffusion combustion phases are computed as well. Comparing these figures shows the effect of load on the heat release rate, combustion duration and in-cylinder pressure. In order to study the part load condition, only the fuel injection timing and the amount of injected mass were changed than those of full load and the rest of the conditions were unaffected. As shown in Figure 4, the peak pressures discrepancy between experiment and computation is less than 0.2%. Increasing load to full load causes in-cylinder peak pressure to increase to 50.2 bar from 42.3 bar and ignition delay decreased to 7.9 CAD from 10.7 CAD with respect to 50% load. It is clear from Figure 5 that at the full load operation, due to injection of fuel in later parts of cycle and also longer injection duration, much of the fuel is burned in diffusion phase. Also Combustion duration at full load operation is longer than that of part load operation. Figure 4 also shows the quantity of computational and experimental results for Start of Combustion (SOC) and Ignition Delay (I.D) crank angle degrees in both loads. The discrepancies of SOC or I.D between computation and experiment at part load and full load operation are as small as 0.8° and 0.1° crank angle respectively. Table 2 also shows a comparison of computational and experimental data for performance parameters of base line engine. It is clear that there are good agreements between them. These agreements between experimental measurements and numerical predictions in the case of baseline engine makes the proposed model a reliable tool to be used for exploring new engine concepts.

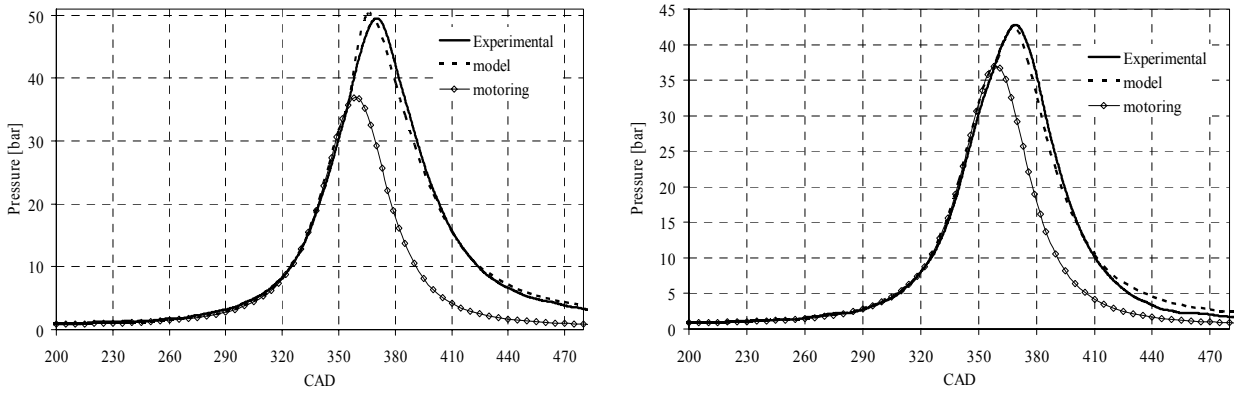

Figure 4. Comparison of measured [40] and calculated pressure for baseline engine at 730 rev. /min for (a) full and (b) part load

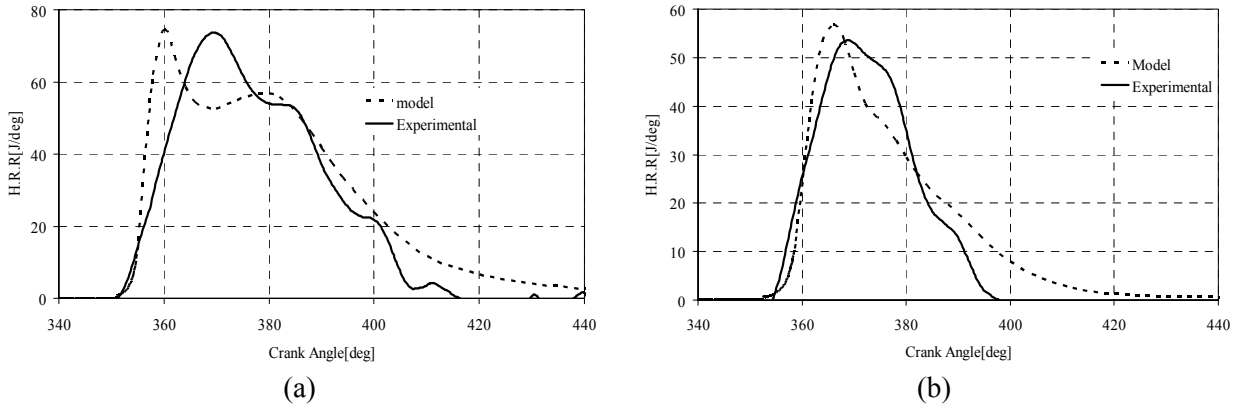

Figure 5. Comparison of experimental [40] and calculated heat release rate for baseline engine at 730 rev. /min for (a) full load (b) part load

At Figures 6 and 7 are shown respectively in-cylinder gas pressure and temperature for base line, adiabatic and adiabatic with 10% EGR at both loads operations. These results show that pressure in the adiabatic without EGR and with 10% EGR cases increase 9 % and 7 % in respect to baseline respectively at full load operating condition. Also it can be observed that in the part load operating condition pressure increases 10 % and 8 % at adiabatic without EGR and with 10% EGR cases respect to baseline respectively. Maximum pressure for baseline, adiabatic without EGR and with 10% EGR cases at full load state are 50.4 bar, 55 bar, and 54.5 bar and those of at pat load are 44, 47.5, 47.5 bar respectively. Peak of pressure for three cases can be observed at 6 degree ATDC. Results for temperatures in cylinder are shown in Figure 7. It is understood from this curve that for the adiabatic case values of peak temperature increase by 230 k and consequently causes that the amount of NO_x emission increases. In part load case maximum temperature for adiabatic condition reaches 1570k and increases by 160k respect to the baseline. It is interesting to see that ignition delay with EGR and without EGR at the adiabatic engine is similar to that of baseline engine. This means that the effect of decreasing oxygen concentration and lower value of γ on ignition delay is equal to the increased charge temperature when the engine is insulated. Also these figures show the effect of load on the cylinder pressure and temperature at constant speed and injection timing. During part load operation as load is increased, more fuel is injected later in the cycle. It can be assumed that the oxygen concentration in the prechamber decreases as more fuel is injected. Therefore, the increases in fuel injection with load may reduce the extent of burning of last portions of fuel injected into the prechamber. The unburned fuel in the prechamber may therefore increase with load, but its burning rate in the main chamber may likewise increase [42, 43]. This is primarily due to higher temperature reached in the main chamber during the expansion stroke, as can be seen in temperature and pressure traces of Figures 6 and 7. Figure 8 shows the behavior of heat release rate for three states at both part and full loads operation. It is clear from this figure that at full load operation combustion period shifts towards expansion stroke, where pressure is lower and total combustion duration gets long. Therefore, at full load operations, combustion starts in the prechamber near 9^0 crank angle after fuel injection and then continuous at the main chamber while at the part load combustion takes place only in prechamber. Also Figure 8 shows a comparison of various heat release rate for both loads. The diagrams clearly show that with proper adjustment of EGR mass fraction at full load operation, it is possible to partially offset the adverse effect of insulation on heat release rate and hence to obtain improved performance and lower NO_x. While the insulation with and without EGR at part load operation does not have considerable effect on the amount of heat release rate. As shown in Figure 9, accumulated heat releases in the adiabatic case is larger than the other cases thus, the amount of burnt fuel in this case is more than the others. Because of shortage of oxygen in the charge of cylinder in the EGR case, amount of burnt fuel and consequently accumulated heat release are less than the others. Figure 10 shows the effect of insulation without and with EGR(EGR =10% rate) on the soot and NO_x emissions in an IDI diesel engine. It can be seen that the NO_x decreased significantly with EGR adding, whereas the soot slowly increased. The effect of insulation and EGR adding on the soot emission is found negligible at part load operation, as show in Figure 10. The results show that production of soot in the both operating loads at the adiabatic condition is lower respect to base line. Reason of this happening is increased cylinder gas temperature due to insulation of engine. Therefore, the effect of insulation in the production of soot is positive. But diagrams for production of NO_x emission in both part and full loads, illustrate that production of NO_x is very high in the adiabatic condition. In the adiabatic case the amount of NO_x is 172 % and 272 % more than baseline respectively in part and full loads and this is the negative effect of temperature increasing in adiabatic case. Adding EGR to the initial charge is suitable method for solving this problem. With this EGR adding to the adiabatic case we obtain lower NO_x even less than baseline engine in both operating loads. But it reduces performance characteristics of engine as power and increases brake specific fuel consumption respect to adiabatic case. At full load operation, Soot emission increases than that of baseline engine while it is not varied at part load operation. As an engine is generally operated for a short time intervals at full load condition, this increment can be omitted when improvements in BSFC and decrease in NO_x is considered together.

Figure 11 represents the evolution of temperature, NO_x and soot emissions at 360, 380, 400 and 420 crank angles for three cases at both part and full load operating conditions. It is clear from Figure 11a that ,at 360°CA , flame propagations (temperature contours) are similar for three cases and combustion started at the upper edge of swirl chamber throat(stoichiometric zone) and then propagated to pre and main chamber at 380°CA . Also the development of the temperature fields at three cases between 360 and 380°CA show that the axial and the radial penetrations of the flame front are almost equal. Thus, the

flame front reaches the lateral cylinder wall and the cylinder wall opposite to the pre-chamber at approximately the same time. It reveals that the flame started in pre-chamber and then invades a large portion of the main-chamber very quickly. Flame distribution which is shown in this figure also indicates that the swirl generated in swirl chamber during the compression stroke becomes gradually weaker due to opposing flow in glow plug channel (don't shown contours). Therefore, at the end of injection period at 380°CA the flame reaches near to injector location without distortion. Also the similar trends are observed for flame temperature distribution at 360°CA and 380°CA. This would result in similar the mixture formation processes for three cases at these crank angles. In the front view at 400°CA, the hot gas from the pre-chamber reaches the opposite side of main chamber. This leads to the formation of two large eddies each occupying a half of the main chamber and staying centered with respect to the two half of the bowl(don't shown contours). At 420°CA, these eddies are larger than that of 400°CA and the eddy formed in right half of bowl is larger than that of left half of bowl. At 400°CA, the shape of high temperature regions for baseline and adiabatic with EGR cases are the same. Also at adiabatic case for 400°CA and 420°CA, these regions more spread out in the main chamber and the values of local peak temperature in cylinder are higher than those of two other cases. After 400°CA, these regions transfer to the main combustion chamber and therefore, at part load operation most of NO_x emission form in the main chamber or transfer to it from prechamber. At the full load operation, the momentum of fuel spray increases because of the increase of injection pressure and the increase of the injected fuel mass due to the increased effective flow area with increased nozzle needle lift. Therefore, as shown in Figure 11d, combustion started earlier at the full load operation because of fast mixture formation. It is clear from this figure that flame can develop in whole of glow plug channel and stagnation zone because of fast mixture formation and high swirl ratio in the prechamber at 380CA and 400°CA for three cases. Also similar trends are observed for flame propagation at other crank angles. At Figures 11b, 11c, 11e, 11f the production of NO_x and soot in the main and prechamber are discussed for three cases at both part and full loads operation. It can be seen from Figure 11b that at 380CA the NO_x is produced in the throat and main chamber for three cases at part load operation. At 400CA and 420CA reducing NO_x quantities in the swirl chamber throat is due convection to the main chamber. Also similar trends are observed for baseline and adiabatic with EGR cases while at the adiabatic cases increase in the global NO mass fractions follow the higher global temperature in cylinder. The main chamber NO formation is much higher than that of swirl chamber at three cases. On the other hand the lower global temperature and the lower heat release, encountered in the swirl chamber of engine, lead to a much lower production of NO_x. As shown in Figure 11e, at 380°CA, the NO forms in the swirl chamber throat, pre and main chambers and then transferred into the main chamber at 400°CA for baseline engine. While at adiabatic without and with EGR cases because of the high temperature in both chambers, the NO emission exist in the pre and main chambers. After the end of injection lean mixture is formed in the upper region of prechamber at adiabatic cases, which with the high temperatures and the slow movement leads to a center of NO formation. At 420°CA most of the NO_x is found in the main chamber.

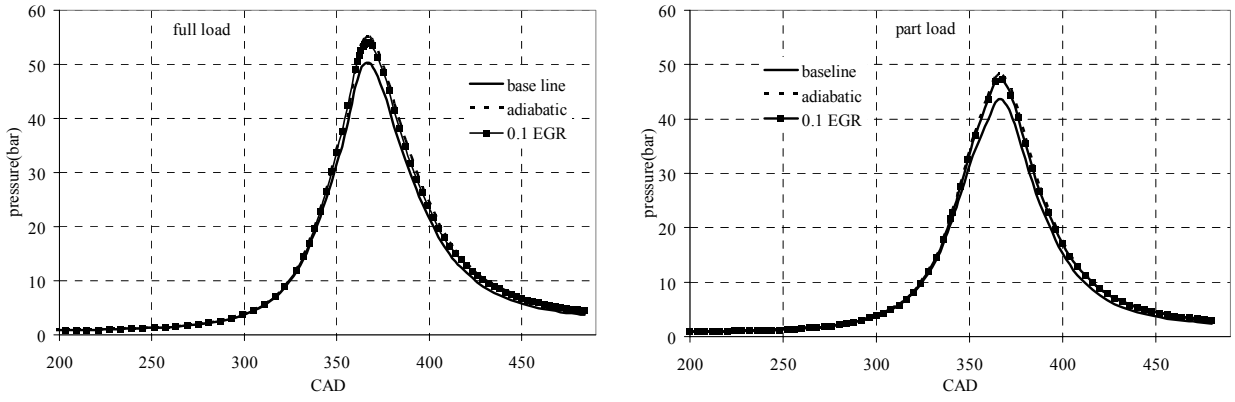

(a) (b)

Figure 6. Comparison of calculated pressure at 730 rev/min at three operating conditions for (a) full and (b) part load

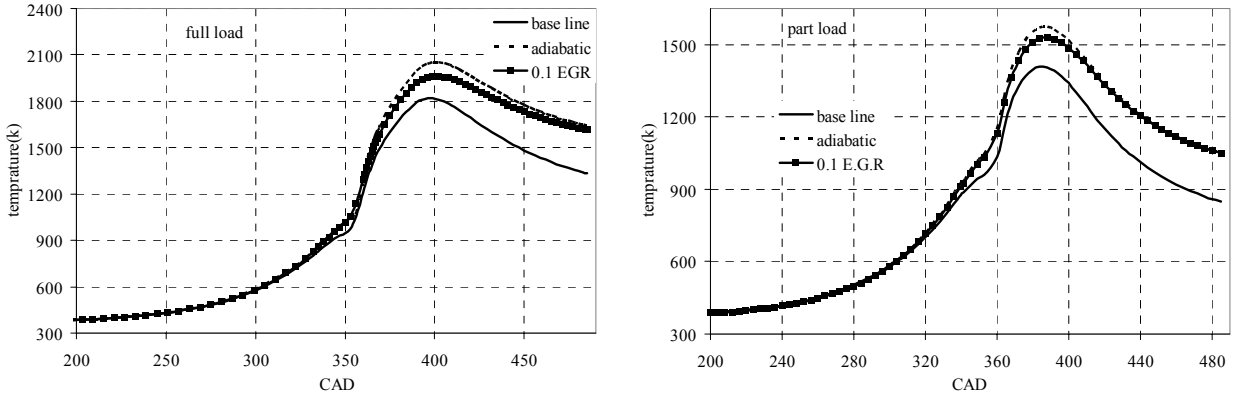

(a) (b)

Figure 7. Comparison of calculated temperature at 730 rev/min at three operating conditions for (a) full and (b) part load

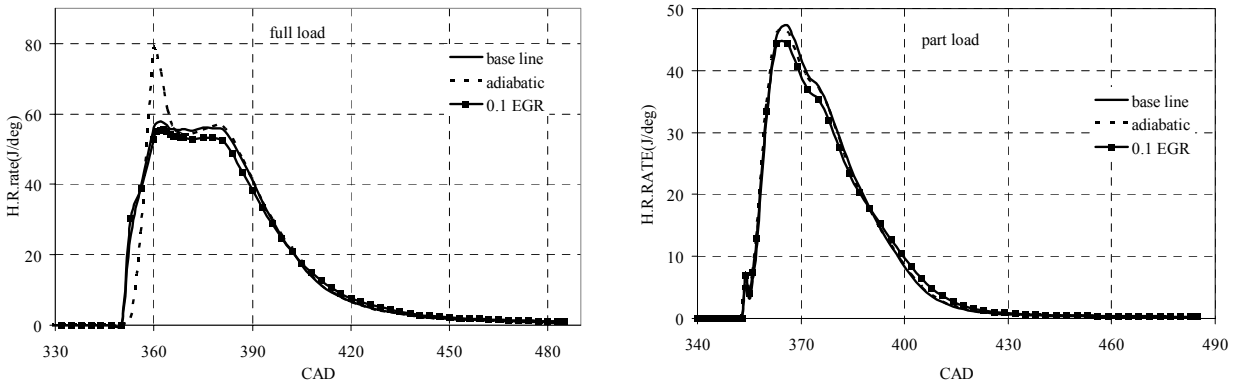

(a) (b)

Figure 8. Comparison of calculated heat release rate at 730 rev/min at three operating conditions for (a) full and (b) part load

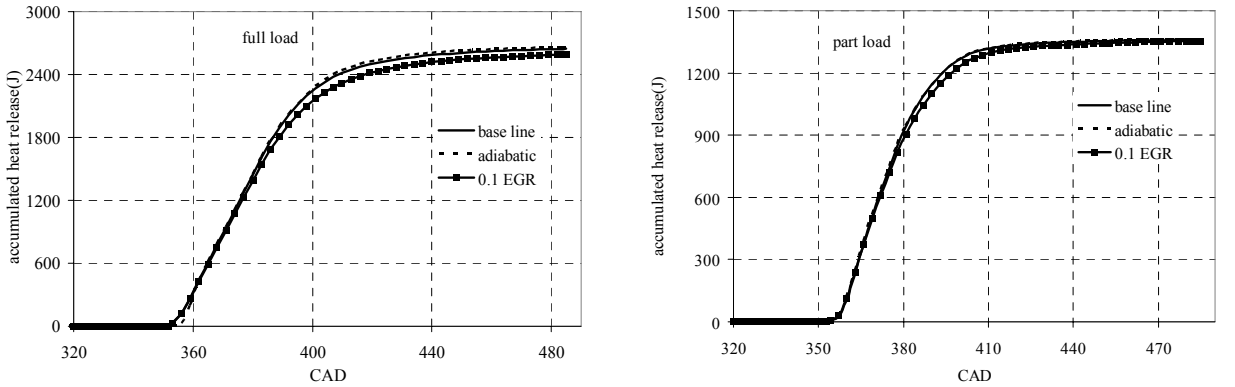

(a) (b)

Figure 9. Comparison of calculated accumulated heat release rate at 730 rev/min at three operating conditions for (a) full and (b) part load

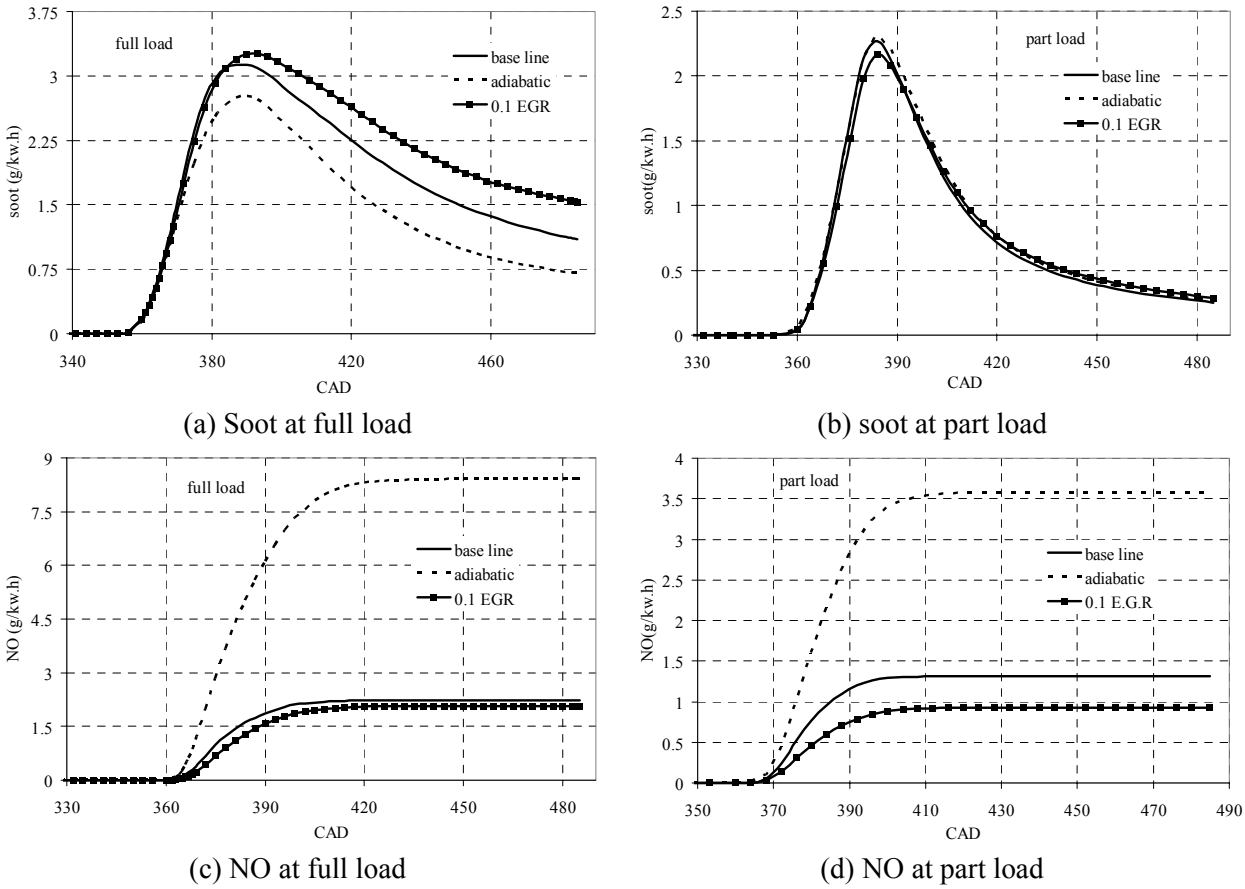

(a) Soot at full load (b) soot at part load

(c) NO at full load (d) NO at part load

Figure 10. (a-d) Comparison of calculated exhaust emissions at 730 rev/min at three operating conditions at full and part loads

Finally in Figures 11c and 11f, we present the evolution of the soot mass in the main and pre chambers for three cases at part and full load operation respectively. As indicated by these figures, in the three cases at part and full load conditions, the main cause of the exhaust smoke is spray-wall impingement which leads to fuel adhesion on the wall and the stagnation of a rich fuel-air mixture. Under part load operation, fuel spray impinges against the chamber wall from the beginning of injection due to the low swirl ratio in swirl chamber. Therefore in Figure 11c, dense soot cloud shown by the white area appears near the spray-wall impinging point from the early stage of the combustion period. Some part of this dense soot flows out to the main combustion chamber just when the initial flame flows out (at 380°CA of three cases, in Figure 11a). This simultaneous flow out is confirmed by the observation of the main combustion chamber that the dense soot appears at almost the same time of the flame (at 380°ATDC of Conventional, in Figures 11a and 11c). As the formation of the dense soot continues throughout the injection period due to the continuous fuel-spray impinging, the dense soot continuously flows out to the main combustion chamber and cannot be fully oxidized. This incomplete oxidation is shown by the fact that the dense soot does not disappear and spreads to the whole area of the main combustion chamber (at 400°CA in Figure 11c) while a part of soot emission remains in glow plug channel because of the stagnation of a rich fuel-air mixture region. At 420°CA, dense soot in the main chamber disappears because of complete oxidation. Also at full load operation, the harder spray impingement than the part load operation causes more fuel adhesion on the wall near this point. This adherent fuel is not quickly evaporated and formed fuel vapor is hardly carried out of this area, because the stagnation zone is formed here due to the chamber shape. Thus, the rich fuel-air mixture stagnates in this zone under the condition of high temperature and insufficient oxygen to form the dense soot cloud. At 360°CA, the soot is produced in regions of high fuel concentrations, when cold fuel is injected into areas of hot gases at upper edge of swirl chamber throat. It is obvious from flame distributions (Figures 11a and 11d) that in the full load operation, the flow field more interact with the spray than in the part load operation. Therefore, at 380°CA, The zones of the soot formation are occurred in the glow plug channel and in the

center of swirl chamber. Similar trends are observed at this crank angle for three cases. At 400°CA, there are two centers of soot production visible in the contour plots, one has attached itself to the glow plug channel opposing wall and the other spreads itself to the whole area of the glow plug channel. At high loads, we observe that the main part of soot formation takes place in the prechamber due to low swirl ratio and the insufficient oxygen mass available. It can be seen from Figures 11a, 11b, 11d and 11e that the NO_x formation in the main chamber is intensified in areas with equivalence ratio close to 1 and the temperature higher than 2000 K. In addition to this, as shown in these figures that the area which the equivalence ratio is higher than 3 and the temperature is approximately between 1600 K and 2000 K yields in greater soot concentration. A local soot-NO_x trade-off is evident in these contour plots where the NO_x and Soot formation occur on opposite sides of the high temperature region.

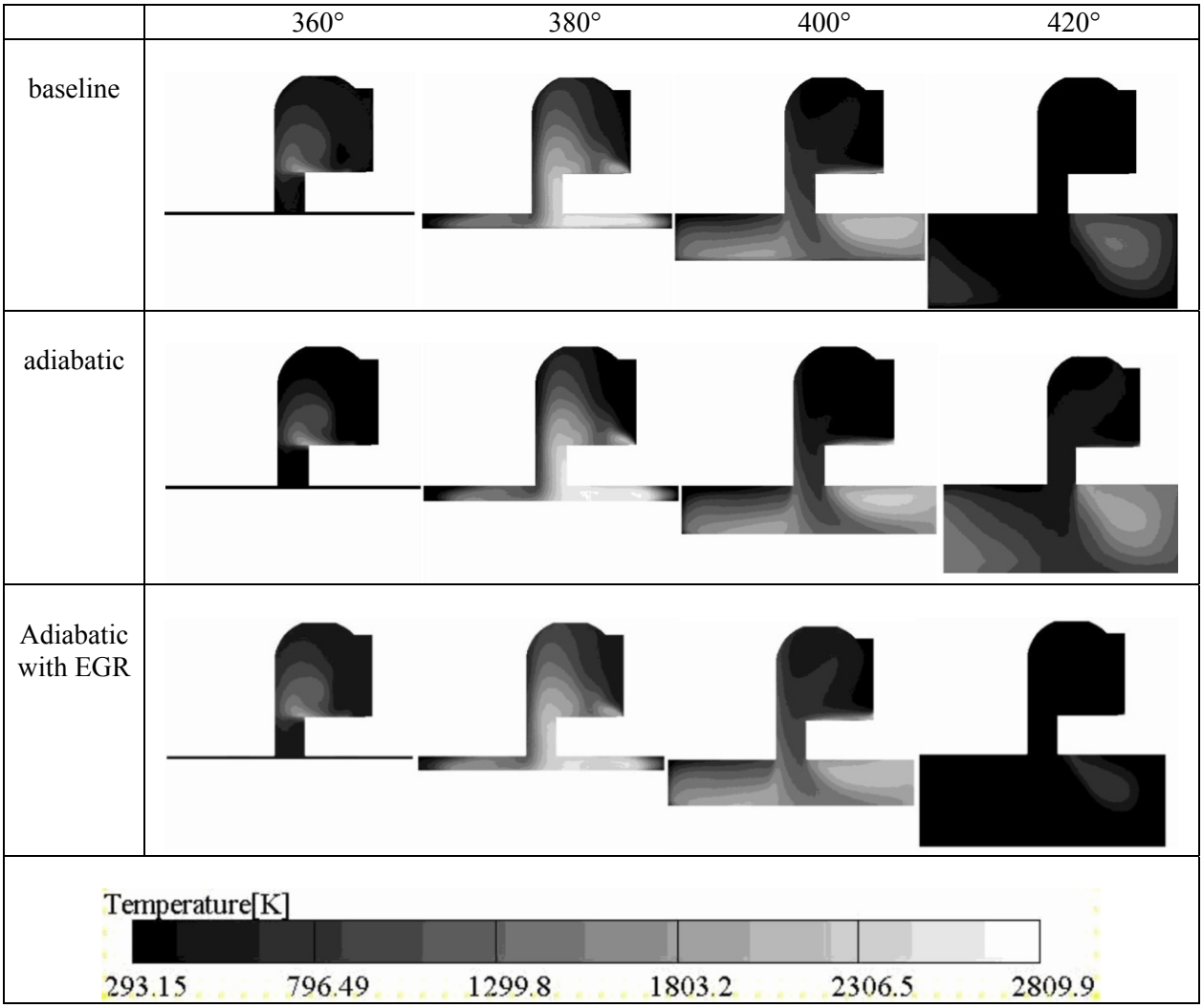

Figure 11. (a) Contour plots of temperature at three cases for part load operation at 360, 380, 400, 420°CA (from left to right)

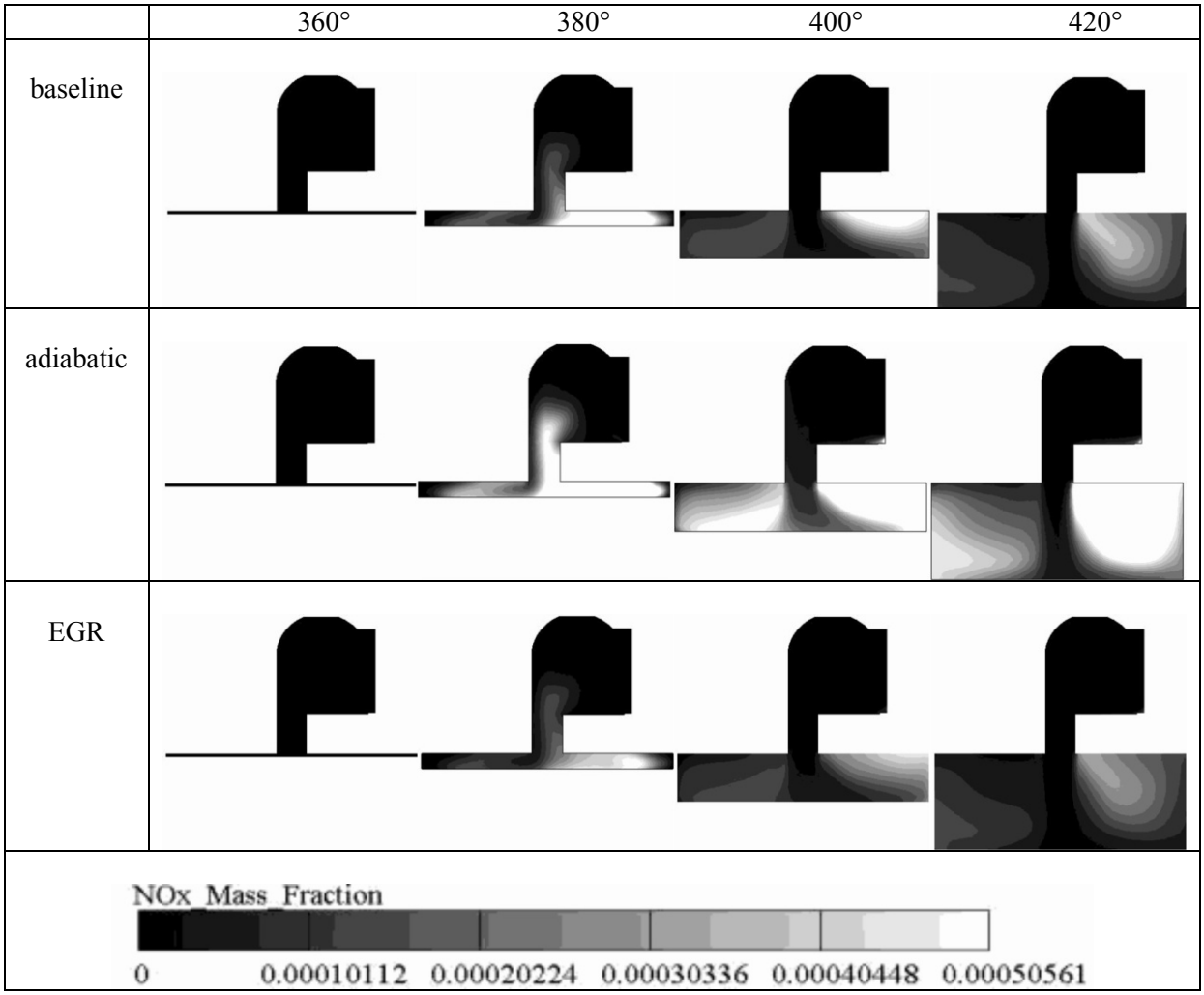

Figure 11. (b) Contour plots of NOx mass fraction at three cases for part load operation at 360, 380, 400, 420°CA (from left to right)

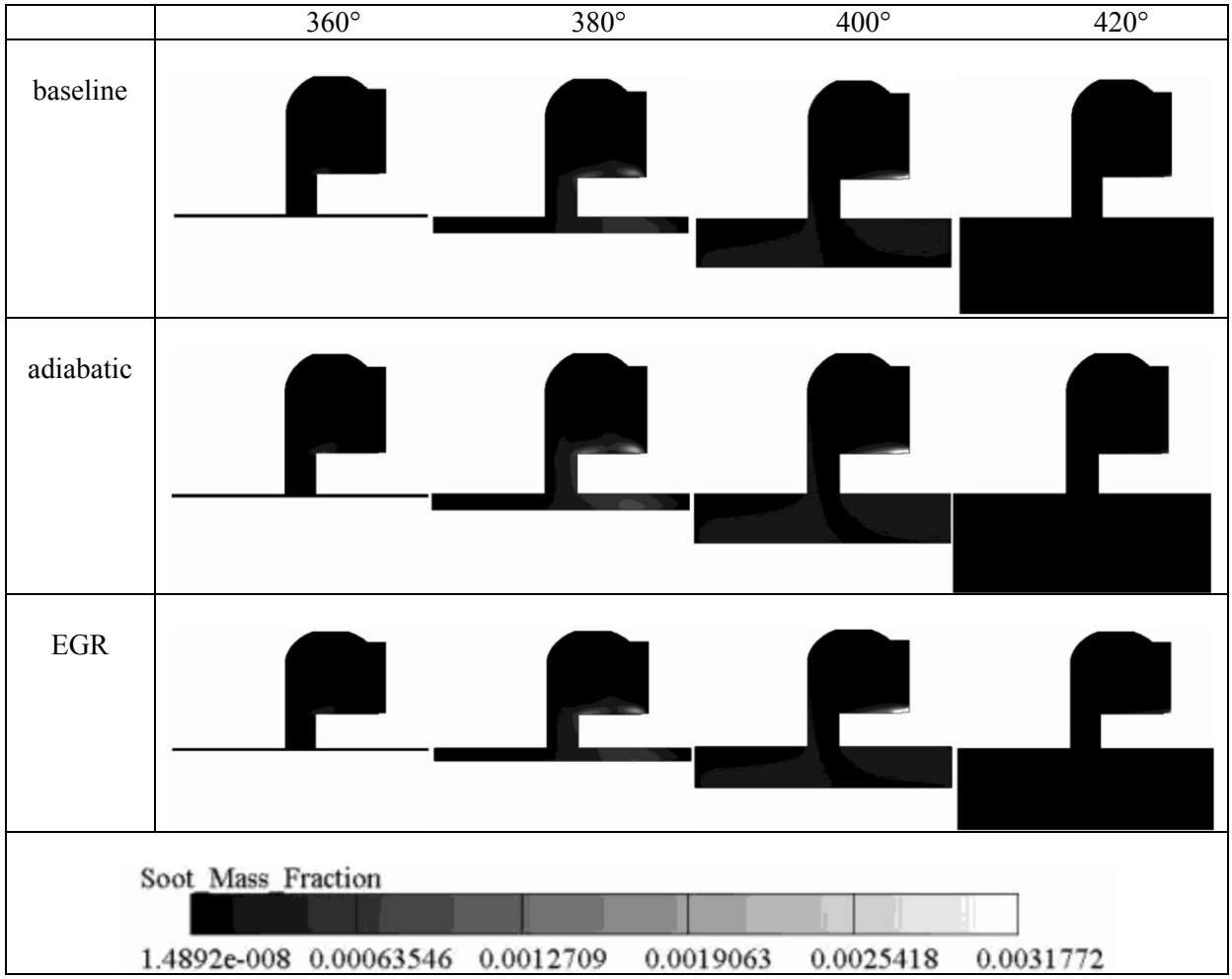

Figure 11. (c) Contour plots of Soot mass fraction at three cases for part load operation at 360, 380, 400, 420°CA (from left to right)

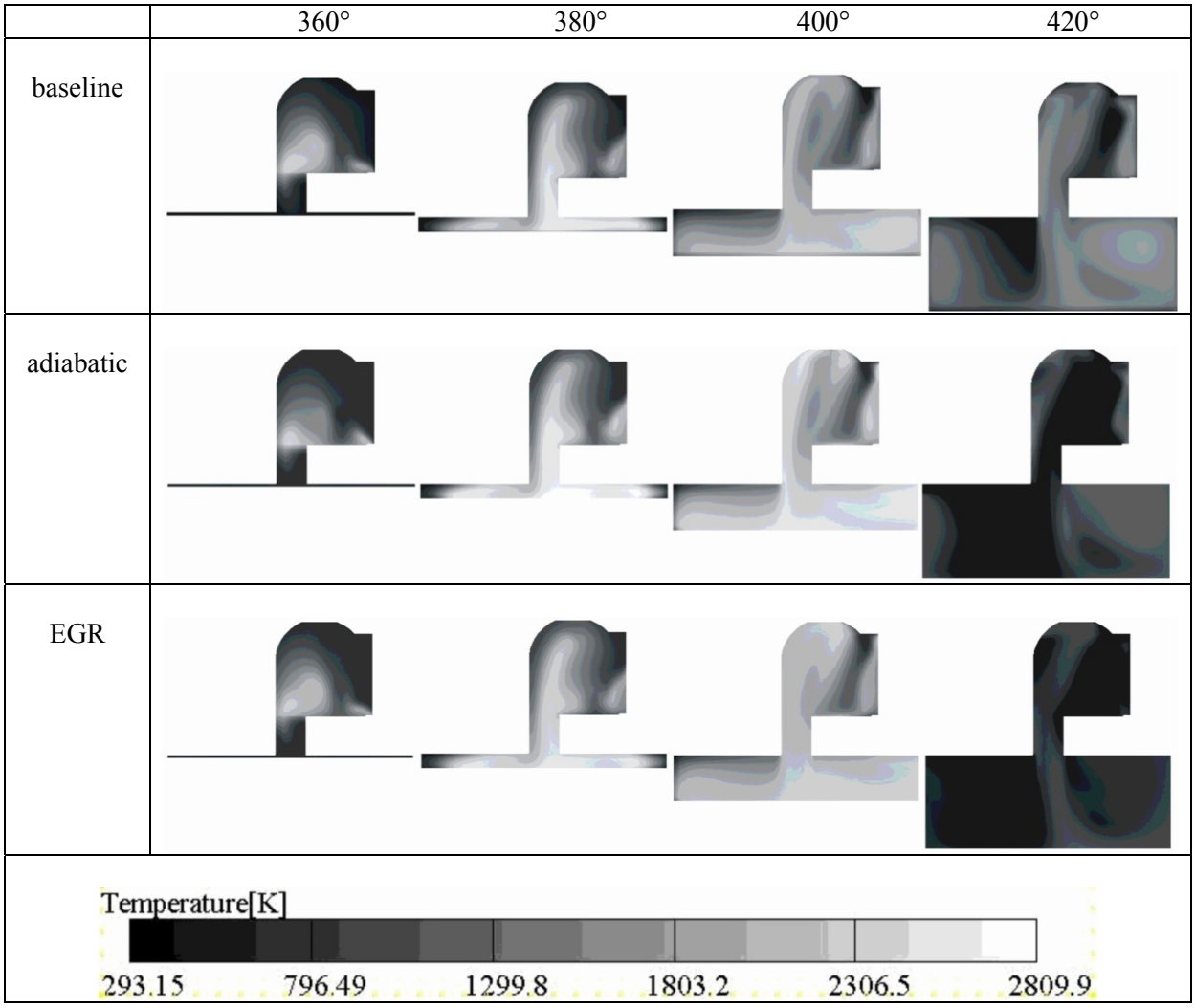

Figure 11. (d) Temperature contour plots at three cases for full load operation at 360, 380, 400, 420°CA (from left to right)

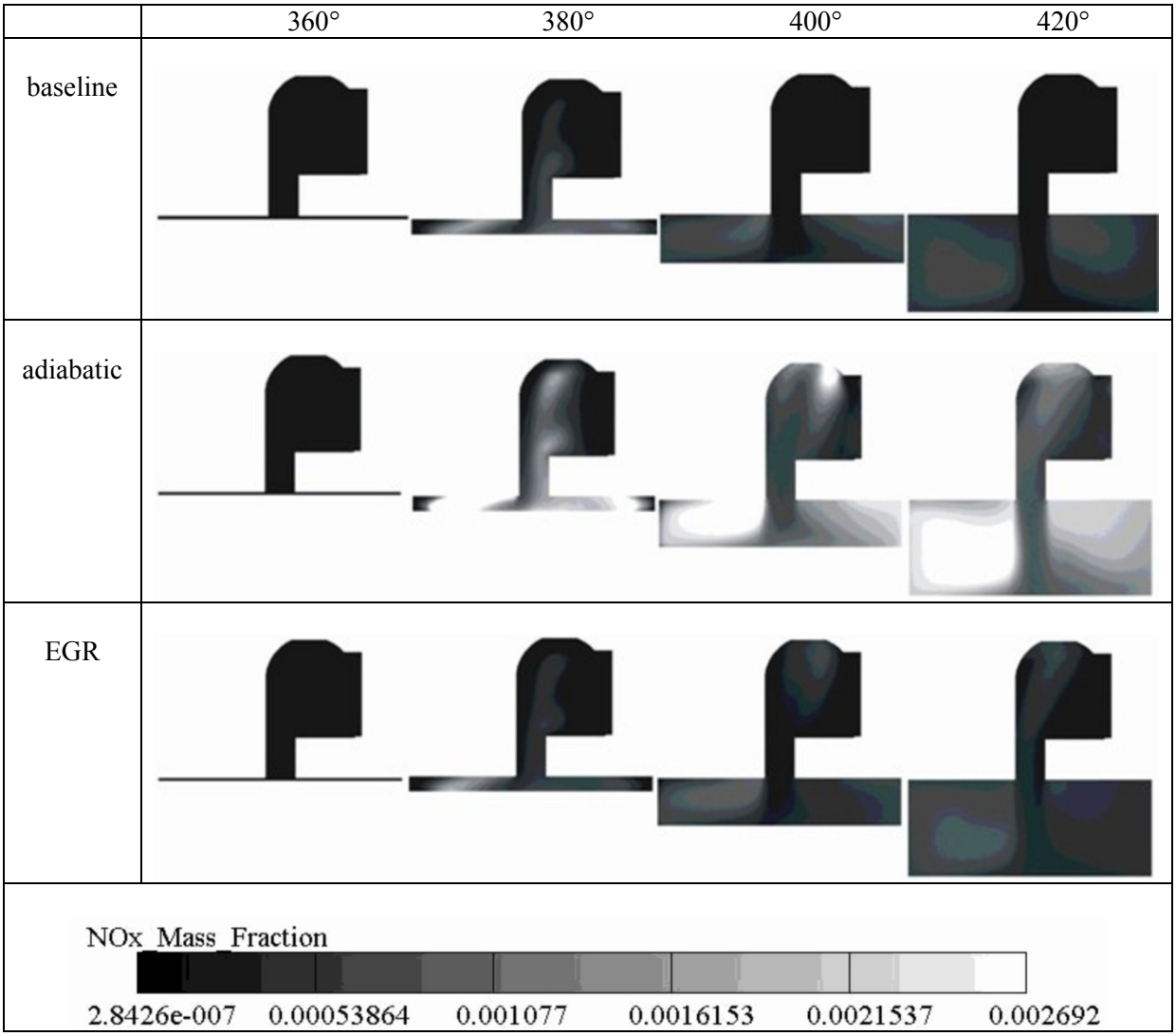

Figure 11. (e) Contour plots of NOx mass fraction at three cases for full load operation at 360, 380, 400, 420°CA (from left to right)

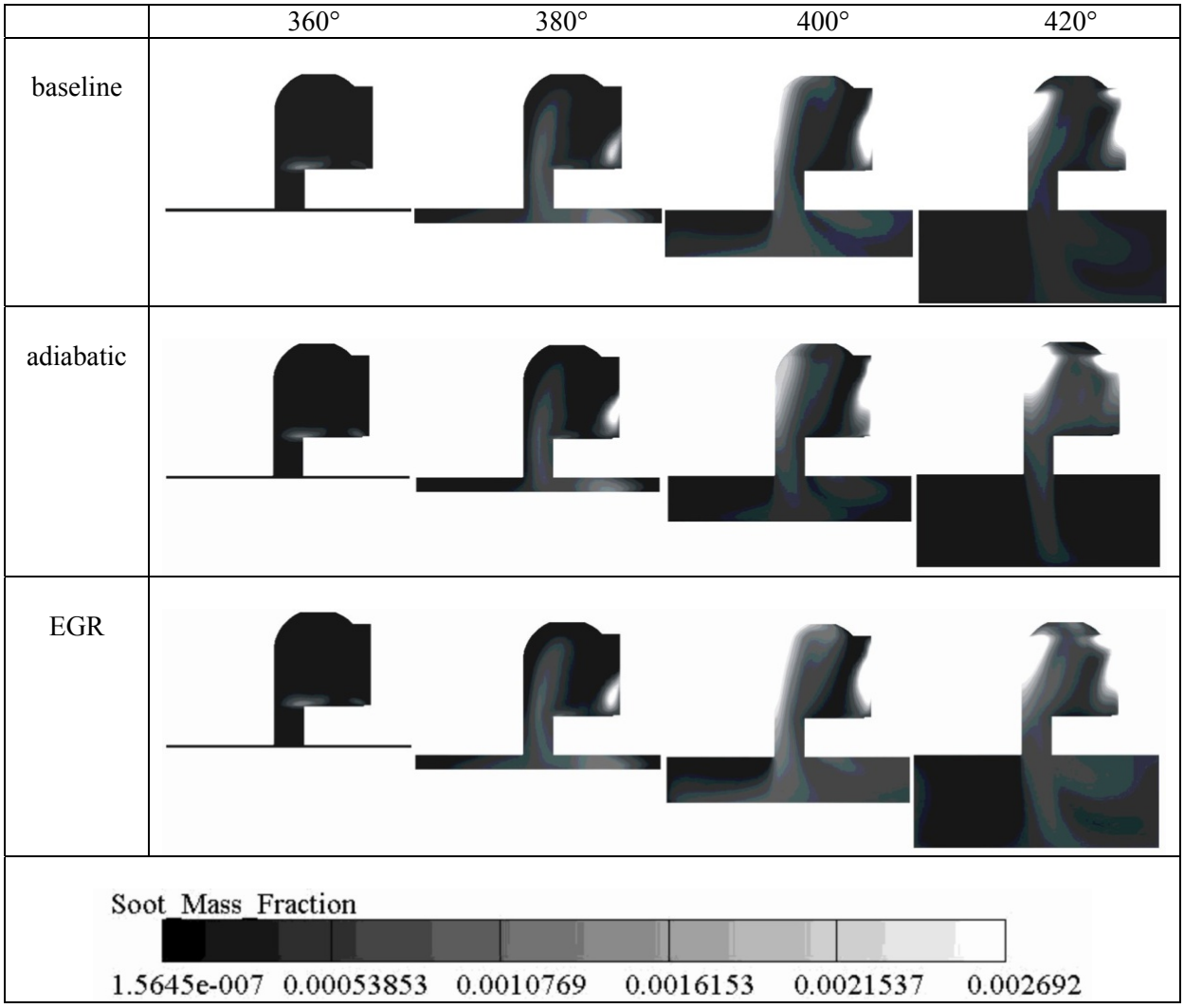

Figure 11. (f) Contour plots of Soot mass fraction at three cases for full load operation at 360, 380, 400, 420°CA (from left to right)

3.1 Performance parameters

In order to analyze the engine performance parameters, the gross indicated work per cycle was calculated from the cylinder pressure and piston displacement, as follows:

$$W = \int_{\theta_1}^{\theta_2} PdV \tag{3}$$

where θ_1, θ_2 are the start and end of the valve-closed period, respectively (i.e. IVC= 15° ABDC and EVO= 55° BBDC).

Also the indicated power per cylinder and indicated mean effective pressure were related to the indicated work per cycle by:

$$P(KW) = \frac{W(N.m)N(rpm)}{60000n} \tag{4}$$

$$IMEP = \frac{W}{V_d} \tag{5}$$

where n=2 is the number of crank revolutions for each power stroke per cylinder, N is the engine speed in rpm and V_d is volume displacement of piston. The brake specific fuel consumption (BSFC) was defined as:

$$BSFC = \frac{\dot{m}_f}{P_b} \tag{6}$$

In Equation (3), the work was only integrated at the part of the compression and expansion strokes; the pumping work has not been taken into account.

Table 3 shows the variation of performance parameters versus load operation at three initial and boundary conditions. By comparison of these parameters, it can be seen that the model predictions have a good accuracy. By insulation of engine, performance characteristics of engine have become better. Also it can be observed that in both operating loads in the adiabatic case BSFC is decreased. Therefore, better fuel economies have been obtained at these states. Also indicated power, indicated mean effective pressure (Imep), and work done per cycle increased in adiabatic case. The amount of BSFC at full and part loads are 18 % and 23 % lower respectively in adiabatic case than baseline and it is the best result of insulation of an IDI diesel engine. The indicated power increased at the adiabatic case 30% and 22.5% in part and full loads respectively. Although in the EGR applying case, performance characteristics of engine are lower than adiabatic case but it is better than baseline and also production of NO_x is less than other cases. When improvement in BSFC and decrease in NO is considered together, in the EGR case we obtain better performance and emission improvement.

Table 3a. Part load

	part load		
	base line	adiabatic with 0.1 EGR	adiabatic
indicated power(kw)	3.04	3.85	3.95
brake power(kw)	2.58	3.27	3.35
Imep(bar)	3.54	4.5	4.6
m fuel (g/sec)	0.196	0.196	0.196
BSFC(g/kw.h)	272.71	215.03	209
work per cycle(J)	499.6	633.62	648.82

Table 3b. Full load

	full load		
	base line	0.1 EGR with 0.1 EGR	adiabatic
indicated power(kw)	5.75	6.75	7.06
brake power(kw)	4.89	5.74	6
Imep(bar)	6.71	7.87	8.23
m fuel (g/sec)	0.391	0.391	0.391
BSFC(g/kw.h)	288	245.65	235
work per cycle(J)	945.76	1109.25	1.16E+03

4. Conclusion

In this paper, a computational study was carried out to investigate the effects of insulation and EGR in an IDI diesel engine. The optimum case for minimum NO_x and soot emissions with improved performance parameters was identified by computational study. Based on this study, the following conclusions are made:

1. The insulation can reduce the soot and isfc, but increase NO_x at part and full load operations.

2. At part load operation, 10% EGR mass fraction rate can significantly reduce the NO_x, and isfc.While the Soot remains relatively unchanged. Therefore optimum EGR mass fraction is equal to 10%.
3. At full load operation, 10% EGR mass fraction rate can significantly reduce the NO_x, but increases the Soot. Also it decreases isfc as well than baseline. It must be noted here that as an engine is generally operated for a short time intervals at full load condition, the increasing soot at this state can be omitted when improvements in BSFC and decrease in NO_x is considered together. This EGR mass fraction is approximately the same as the result of measurements that have been performed by Yoshihiro Hotta et al. [44] and showed during the range of EGR rate from 4% to 8%, simultaneous reduction of soot and NO_x.

References

[1] Canakci, M. Bioresour. Technol. 2007, 98, 1167–1175.
[2] Ozsezen, A. N.; Canakci, M.; Sayin, C. Energy Fuels 2008, 22, 1297–1305.
[3] Ghojel, J.; Honnery, D. Appl. Therm. Eng. 2005, 25, 2072–2085.
[4] Heywood, J. B. Internal Combustion Engine Fundamentals; McGraw Hill International Editions: New York, 1988; pp 491-497.
[5] Bosch Handbook. Diesel-Engine Management: An OverView; Robert Bosch GmbH: Stuttgart, Germany, 2003; pp 24-27.
[6] Owen, K.; Coley, T. Automotive Fuels Reference Book; SAE: Warrendale, PA, 1995; p 375.
[7] Abdel-Rahman, A. A. Int. J. Energy Res. 1998, 22 (6), 483–513.
[8] Iwazaki, K.; Amagai, K.; Arai, M. Energy 2005, 30, 447–459.
[9] Rakopoulos, C. D.; Antonopoulos, K. A.; Rakopoulos, D. C.; Giakoumis, E. G. Appl. Therm. Eng. 2006, 26 (14-15), 1611–1620.
[10] R. Kamo, W. Bryzik, Cummins adiabatic engine program, SAE paper, no. 83314, 1983.
[11] R. Kamo, M. Woods, T. Yaamuda, M. More, " Thermal barrier coating for diesel engine piston, ASME Transactions", paper 80-DGP-14, 1980.
[12] R.H. Thring, "Low heat rejection engines", SAE paper, no. 860314, 1986.
[13] A. Parlak, H. Yasar, B. Sahin, "Performance and exhaust emission characteristics of a lower compression ratio LHR diesel engine", Energy Conversion & Management 44 (2003) 163–175.
[14] A. Parlak, B. Sahin, H. Yas_ar, "Performance optimization of an irreversible dual cycle with respect to pressure ratio and temperature ratio—an experimental results of a ceramic coated IDI diesel engine", Energy Conversion & Management 45 (7–8) (2004) 1219–1232.
[15] R. Kamo, W. Bryzik, "Adiabatic turbo compound engine program", SAE paper, no. 810070, 1981.
[16] F.J. Wallace, J.B. Way, H. Vallmert, " Effect of partial suppression of heat loss of coolant on the high output diesel engine cycle", SAE paper, no. 790823, 1979.
[17] D.A. Parker, G. Donison, "The development of an Air gap Insulated Piston",SAE paper, no. 870652, 1985.
[18] R. Kamo, N.S. Mavinahally, L. Kamo, W. Bryzik, R. Schwartz, " Injection Characteristics that Improve Performance of Ceramics Coated Diesel engines",Society of Automotive Engineers, 1999.
[19] Adnan Parlak, Halit Yasar, Can Hasimogˇlu, Ahmet Kolip, "The effects of injection timing on NOx emissions of a low heat rejection indirect diesel injection engine", Applied Thermal Engineering 25 (2005) 3042–3052.
[20] Ekrem Buyukkaya , Muhammet Cerit, "Experimental study of NOx emissions and injection timing of a low heat rejection diesel engine", International Journal of Thermal Sciences 47 (2008) 1096–1106.
[21] D.W. Dickey,"the effect of insulated chamber surfaces on direct injected diesel engine performance, emissions, and combustion", SAE paper, no. 890292, 1989.
[22] S. Jaichandar and P. Tamilporai, "The Status of Experimental Investigations on Low Heat Rejection Engines", SAE paper 2004-01-1453.
[23] C.A. Amann, Promises and challenges of the low-heat-rejection diesel, Journal of Engineering for Gas Turbines and Power 110 (1988) 475–481.
[24] Yiming Wang, Changlin Yang, Guocai Shu, Yincheng Ju, and Kuihan Zhao, "An Observation of High Temperature Combustion Phenomenon in Low-Heat- Rejection Diesel Engines", SAE paper, no. 940949, 1994.
[25] Dennis Assanis and Kevin Wiese, Ernest Schwarz and Waiter Bryzik , "The Effects of Ceramic Coatings on Diesel Engine Performance and Exhaust Emissions", SAE paper no. 910460, 1991.

[26] Adnan Parlak, "The effect of heat transfer on performance of the Diesel cycle and exergy of the exhaust gas stream in a LHR Diesel engine at the optimum injection timing", Energy Conversion and Management 46 (2005) 167–179.
[27] T. Hejwowski, A. Weronski, "The effect of thermal barrier coatings on diesel engine performance", Vacuum 65 (2002) 427.
[28] K. Toyama, T. Yoshimitsu, T. Nishiyama, "Heat insulated turbo compound engine",SAE Transactions, vol. 92, 1983, p. 3.1086.
[29] Arash Nemati, Shahram Khalilarya, Samad Jafarmadar, Hassan Khatamnejhad, Vahid Fathi. Numerical parametric investigation of a gasoline fuelled partially-premixed compression-ignition engine. International Journal of Energy and Environment 201, 2(4); 739-748.
[30] P. Pinchon, "Three dimensional modeling of combustion in a pre-chamber Diesel engine", SAE 890666.
[31] M. Zellat, Th. Rolland and F. Poplow, "Three dimensional modeling of combustion and soot formation in an indirect injection diesel engine", SAE 900254.
[32] Tim Sebastian Strauss, George Wolfgang Schweimer, "Combustion in a swirl chamber diesel engine simulation by computation of fluid dynamics", SAE 950280.
[33] AVL FIRE user manual V. 8.5; 2006.
[34] Han Z., Reitz R. D., "Turbulence Modeling of Internal Combustion Engines Using RNG K-e Models", Combustion Science and Technology, Vol. 106, pp.267-295., 1995.
[35] Liu AB, Reitz RD., "Modeling the effects of drop drag and break-up on fuel sprays", SAE Paper NO. 930072; 1993
[36] Dukowicz JK., "Quasi-steady droplet change in the presence of convection", informal report Los Alamos Scientific Laboratory", LA7997-MS.
[37] Gosman AD, Ioannides E (1981), "Aspects of Computer Simulation of Liquid-Fueled Combustors", AIAA paper no 81-0323
[38] Naber JD, Reitz RD., "Modeling engine spray/wall impingement", SAE Paper NO. 880107, 1988.
[39] Halstead M, Kirsch L, Quinn C., "The Auto ignition of hydrocarbon fueled at high temperatures and pressures - fitting of a mathematical model", Combustion Flame 30 (1977): 45-60.
[40] A. Mohammahi Kusha, "Ignition of dual fuel engines by using free radicals existing in EGR gases", PhD thesis, Faculty of mechanical engineering, Tabriz university, Iran 2008.
[41] Patterson M. A., Kong S. C., Hampson G. J. Reitz R. D., "Modeling the Effects of Fuel Injection Characteristics on Diesel Engine Soot and NOx Emissions", SAE Paper 940523, 1994.
[42] Patterson, D.J., Henein, N.A "Emission from combustion Engine and their control", Ann Arbor Science Publisher INO 1972
[43] Carsten Baumgarten, "Mixture formation in internal combustion engines", Springer publications 2006.
[44] Yoshihiro Hotta et al., "Combustion Improvement for Reducing Exhaust Emissions in IDI Diesel Engine", SAE Paper 980503, 1998.

Syed Yousufuddin received his M.Tech in Thermal Engineering from Jawaharlal Nehru Technological University, Hyderabad,India in 1997 and Ph.D in IC Engines from Osmania University, Hyderabad, India in January 2009. He is presently working as a faculty in the department of Mechanical Engineering at Jubail University, Jubail, Saudi Arabia. He also worked as a Professor and Head of department in the Department of Mechanical Engineering, Vidya Vikas Institute of Technology, Andhra Pradesh, India. He has 14 years of teaching and research experience. He has nine papers in International journals and has presented and published 17 papers in International (ASME) and National Conferences. He has authored a text book on Thermodynamics which was published by Sure Publications, India. His research interest includes alternate fuels, modern trends in IC engines and hybrid vehicles. He is a reviewer for International Journal of Engineering, Iran and Hydrogen Energy Journal.
E-mail address: syedyousufuddin@rediffmail.com

K.Venkateswarlu received his M.Tech in Thermal Engineering from Jawaharlal Nehru Technological University, Hyderabad, India in 2006 and pursuing Ph.D in IC Engines from, Jawaharlal Nehru Technological University, Kakinada, India (Registered 2010). He is presently working as a faculty in the department of Mechanical Engineering at K.L University, Guntur, Andhra Pradesh, India . He has 14 years of teaching experience. He has one paper in national journal and has presented and published one paper in National Conference. His research interest includes alternate fuels for IC engines and fuel efficiency improvement of diesel engines. Mr. K.Venkateswarlu is a member of Society of Automotive Engineers (Membership number: 110410222)(Valid upto June 2012).
E-mail address: Chaitu9903@yahoo.co.in

Naseeb Khan obtained his Bachelors in Mechanical Engineering and Master's in Industrial Engineering from Jawaharlal Nehru Technological University, Hyderabad, India. He is presently pursuing his Ph.D in I.C Engines from Jawaharlal Nehru Technological University, Hyderabad, India. He is working as Assistant Professor in the department of Mechanical Engineering at Shaaz College of Engineering. & Technology, Ranga Reddy (District), Andhra Pradesh, India. He has published 2 papers in international journals. Mr. Naseeb Khan is a Life Member of Indian Society of Technical Education (ISTE)-(LM 67990) and Associate Member of Institution of Engineers, India (AIE). (A-550341-9).
E-mail address: mrnaseebkhan@gmail.com